Spin excitations and quantum criticality in the quasi-one-dimensional Ising-like ferromagnet CoCl_{2}·2D_{2}O in a transverse field

J. Larsen, T. K. Schäffer, U. B. Hansen, S. L. Holm, S. R. Ahl, R. Toft-Petersen, J. Taylor, G. Ehlers, J. Jensen, H. M. Rønnow, K. Lefmann, and N. B. Christensen

Spin Excitations and Quantum Criticality in the Quasi One-Dimensional Ising-Like Ferromagnet CoCl₂ · 2D₂O in a Transverse Field

J. Larsen,[1] T. K. Schäffer,[2] U. B. Hansen,[2] S. L. Holm,[2] S. R. Ahl,[1, 2] R. Toft-Petersen,[1, 3]

J. Taylor,[4] G. Ehlers,[5] J. Jensen,[6] H. M. Rønnow,[7] K. Lefmann,[2] and N. B. Christensen[1]

[1]*Department of Physics, Technical University of Denmark, 2800 Kgs. Lyngby, Denmark*
[2]*Nanoscience Center, Niels Bohr Institute, Universitetsparken 5, 2100 Copenhagen Ø, Denmark*
[3]*Helmholtz Center for Energy and Materials, 14109 Berlin Wannsee, Germany*
[4]*European Spallation Source ERIC, Data Management and Software Center,*
Ole Maaløes vej 3, 2200 Copenhagen N, Denmark
[5]*Quantum Condensed Matter Division, Oak Ridge National Laboratory, Oak Ridge, Tennessee 37830, USA*
[6]*Niels Bohr Institute, Universitetsparken 5, 2100 Copenhagen Ø, Denmark*
[7]*Laboratory of Quantum Magnetism, Ecole Polytechnique Federale Lausanne, Switzerland*
(Dated: October 12, 2017)

We present experimental evidence for a quantum phase transition in the easy-axis $S = 3/2$ anisotropic quasi one-dimensional ferromagnet CoCl₂ · 2D₂O in a transverse field. Elastic neutron scattering shows that the magnetic order parameter vanishes at a transverse critical field $\mu_0 H_c = 16.05(4)$ T, while inelastic neutron scattering shows that the gap in the magnetic excitation spectrum vanishes at the same field value, and reopens for $H > H_c$. The field dependence of the order parameter and the gap are well described by critical exponents $\beta = 0.45 \pm 0.09$ and $z\nu$ close to $1/2$, implying that the quantum phase transition in CoCl₂ · 2D₂O differs significantly from the textbook version of a $S = 1/2$ Ising chain in a transverse field. We attribute the difference to weak but finite three-dimensionality of the magnetic interactions.

I. INTRODUCTION

Quantum phase transitions (QPT's)[1] have emerged as a major theme in experimental[2–5] and theoretical[1,6] studies of condensed matter physics. The simplest QPT occurs in the transverse field Ising chain (TFIC) model describing an isolated chain of ferromagnetically coupled $S = 1/2$ spins in a transverse magnetic field[7]

$$\mathcal{H}_{\mathrm{TFIC}} = -J \sum_i \left[S_i^z S_{i+1}^z + (\lambda/2) S_i^x \right], \qquad (1)$$

where $J > 0$. At $T = 0$ and zero applied field, $\lambda = 0$, the ferromagnetic exchange interactions cause the chain to polarize, leaving two possible ground states $\Pi_{i=1}^N |\uparrow\rangle_i$ or $\Pi_{i=1}^N |\downarrow\rangle_i$. Here, the states $|\uparrow\rangle_i$ and $|\downarrow\rangle_i$ are the $m_S = \pm 1/2$ eigenstates of S_i^z. Application of a transverse field, $\lambda > 0$, mixes the $|\uparrow\rangle_i$ and $|\downarrow\rangle_i$ states, eventually leading to the disappearance of long-range order at $\lambda = 1$[1]. The transverse field parameter is $\lambda = H/H_c$, where the critical field is given by $g\mu_B\mu_0 H_c = J/2$, a factor of 2 smaller than the value determined in the mean-field approximation[7]. The ground state in the high-field limit, $\lambda \gg 1$, is qualitatively different. In this so-called quantum paramagnetic phase all spins are parallel to the applied field, $\Pi_{i=1}^N |\rightarrow\rangle_i$ with $|\rightarrow\rangle_i = (|\uparrow\rangle_i + |\downarrow\rangle_i)/\sqrt{2}$. The spin excitations at $\lambda = 0$ are propagating domain walls while for high fields, they derive from single spin-flips and are similar to conventional ferromagnetic spin waves. Diagonalization of Eq. (1) for $H < H_c$[1,7] yields a spectrum $\hbar\omega(Q) = (J/2)\sqrt{1 + \lambda^2 - 2\lambda\cos(Q)}$ with a $Q = 0$ excitation gap closing as $\Delta = J(H_c - H)/2H_c$ upon approaching H_c from below. For an ideal TFIC, the expectation therefore is $\Delta \propto (H_c - H)^{z\nu}$ with $z\nu = 1$.

To date there exists no fully satisfactory direct experimental test of this prediction for the field dependence of the excitation gap in materials that can be approximated by Eq. (1). One exhaustively studied candidate compound is the columbite CoNb₂O₆[8,9], which is comprised of chains of ferromagnetically coupled effective $S = 1/2$ ions, with neighboring chains coupled to each other by weak antiferromagnetic interactions. In this material, however, the Bragg peaks characteristic of 3D long-range magnetic order occur with finite interchain wavevector components and only a partial softening of the excitations was observed in Ref.[8]. More generally, if the field-dependence of the gap Δ can be tracked through H_c in a given material, it is interesting to inquire how deviations from the idealized Hamiltonian, Eq. (1), will affect critical exponents.

In this article, we present a neutron scattering study of the salt CoCl₂ · 2D₂O that belongs to the same class of materials as CoNb₂O₆, i.e. compounds consisting of weakly coupled effective $S = 1/2$ ferromagnetic chains with significant exchange anisotropy. Our experimental results demonstrate, for the first time for a material in this class, the theoretically expected complete closure of the excitation gap at the quantum critical transverse field, which in CoCl₂ · 2D₂O is $H_c = 16.05(4)$ T. Quantitatively, we find that the critical exponents characterizing the field-dependence of the Bragg peak intensities and the excitation gap differ significantly from the predictions related to the ideal TFIC model, Eq. (1).

II. THE CHAIN SYSTEM

CoCl$_2\cdot$2D$_2$O crystallizes in the monoclinic space group C$_{2/m}$ with lattice parameters $a = 7.256$ Å, $b = 8.575$ Å, $c = 3.554$ Å and monoclinic angle $\beta = 97.55°$. The structure consists of chains of Co^{2+} ions along the c axis, coordinated by Cl$^-$ ions in the ac-plane. Magnetic ions on different chains are separated by D$_2$O molecules[10]. In the zero-field magnetic structure below $T_N = 17.2$ K all Co^{2+} spins are oriented along the b axis, and spins on neighboring chains are antiparallel[11,12], see Fig. 1. High-field magnetization data[13] reveal a pronounced anisotropy in the saturation field which attains its minimum value $\mu_0 H_c \approx 16$ T for a field-direction transverse to the easy b axis and parallel to the longest Co-Cl bond. In terms of Eq. (1), this defines the transverse field direction, x, in a coordinate system[14] where z is along the b axis.

The ground state term of the Co^{2+} ion has $L = 3$ and $S = 3/2$. The strong crystal field due to the coordinating Cl$^-$ ions and D$_2$O molecules removes the orbital degeneracies leaving a non-degenerate L ground state, whose four corresponding spin states form two Kramers doublets due to the spin-orbit coupling. Neglecting all states apart from the ground state doublet of the Co^{2+} ions, i.e. within an effective $S = 1/2$ approximation, the realistic Hamiltonian for CoCl$_2 \cdot$2D$_2$O in a transverse field becomes

$$\mathcal{H}= -\sum_{i,\alpha,\gamma} \mu_B \mu_0 H^\alpha g_{\alpha\gamma} S_i^\gamma - \tfrac{1}{2}\sum_{i,\delta}\big[J_\delta^z S_i^z S_{i+\delta}^z + \quad (2)$$
$$\tfrac{J_\delta^\perp}{2}\big(S_i^+ S_{i+\delta}^- + S_{i+\delta}^+ S_i^-\big) + \tfrac{J_\delta^a}{2}\big(S_i^+ S_{i+\delta}^+ + S_{i+\delta}^- S_i^-\big)\big].$$

Within this approximation, the original isotropic spin-exchange interaction obtains an Ising-like anisotropy quantified by $J_\delta^\perp = \tfrac{1}{2}\big(J_\delta^x + J_\delta^y\big)$ and $J_\delta^a = \tfrac{1}{2}\big(J_\delta^x - J_\delta^y\big)$ due to the orbital modifications of the spin states. The Cartesian components, H^α, of the applied magnetic field couple to the spins through a second rank tensor g which contains diagonal coefficients g_{xx}, g_{yy} and g_{zz} and zeroes elsewhere. The view of Co^{2+} as an effective $S = 1/2$ ferromagnetic Ising chain was generally accepted, when magnon bound states were observed by Date and Motokawa in the microwave regime[15] and by Torrance and Tinkham in the far-infrared regime[16,17]. The g factors to be presented in Ref.[18] are $g_{xx} = 3.51$, $g_{yy} = 1.94$, and $g_{zz} = 6.60$ consistent with those derived by Narath from susceptibility measurements[14]. The typical energy scale[18] for the interaction along the chain is $J_0^z \simeq 3.4$ meV with anisotropy constants $J_0^\perp \simeq 0.25 J_0^z$ and $J_0^a \simeq 0.1 J_0^z$.

III.   EXPERIMENTAL RESULTS

In the neutron scattering experiments we employed the triple axis spectrometers RITA-II (SINQ, Switzerland) and FLEXX (HZB, Germany) with final neutron energy $E_f = 5$ meV and Be-filters in the scattered neutron beam to remove higher-order contamination. The orientation

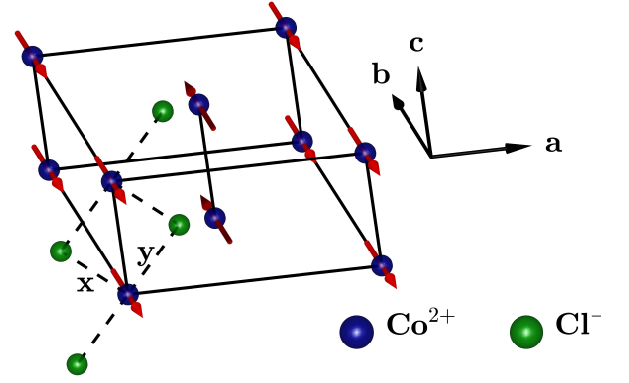FIG. 1. The zero field magnetic unit cell of CoCl$_2 \cdot$ 2D$_2$O. Co^{2+} spins align ferromagnetically along **b** in chains along **c**. Spins on neighboring chains are antiferromagnetically aligned. **x** and **y** represent Co-Cl bond directions, and the easy and hard axes of magnetization in the (**a**, **c**)-plane, respectively[13]. D$_2$O molecules are omitted for clarity. In our experiments, the magnetic field was applied along **x**.

and quality of the solution-grown crystals was checked by X-ray and neutron diffraction. The samples were aligned so that the horizontal scattering plane was spanned by the $(2\,0\,1)$ and $(0\,1\,0)$ reciprocal space directions making the x axis nearly vertical[19]. For the RITA-II experiment, we used a ~ 1 g sample and a 15 T vertical field cryomagnet. The setup at FLEXX was similar, with a ~ 0.25 g sample enclosed in a Dy-booster, adding extra 2.3 T and bringing the maximum field to 17.3 T$> \mu_0 H_c$.

Figure 2(a) shows examples of rocking curve scans around the $\mathbf{Q}_{\mathrm{AFM}} = (2\,1\,1)$ magnetic Bragg peak position. The data were obtained at 1.5 K, and clearly illustrate the disappearance of antiferromagnetic order in the quantum paramagnetic state. The peak lineshape is slightly asymmetric due to the mosaic spread of the sample, but it is field-independent and can be effectively fitted by two Gaussians with fixed positions, widths and intensity ratios. The field-dependence of the square root of the integrated intensity which is proportional to the ordered sublattice moment per ion, $\langle S^z \rangle$, is consistent with a second order phase transition, see Fig. 2(b). We fitted the data to a power law $\langle S^z \rangle \propto (H_c - H)^\beta$ for fields $\mu_0 H > 13$ T and found a critical exponent $\beta = 0.45(9)$. The fitted critical field $\mu_0 H_c = 16.05(4)$ T is in agreement with the value reported in Ref.[13].

We now turn to the excitations in the antiferromagnetically ordered phase. Prior work[20–22] has established that the zero-field response consists of two spin wave branches. The modes of energy $\hbar\omega_x(Q)$ and $\hbar\omega_y(Q)$ are linearly polarized along the **x** and **y** axes, respectively, and their intensities are proportional to the product of g_{xx}^2 (g_{yy}^2) and the sine squared of the angle between $\mathbf{Q}$ and the **x** (**y**) directions[20,22]. In zero field only a single sharp excitation is observed at $\hbar\omega \simeq 3.7$ meV. At the reciprocal lattice point (2 1 1), the small angular separation of 16° between $\mathbf{Q}_{\mathrm{AFM}}$ and the **y** axis, in combination
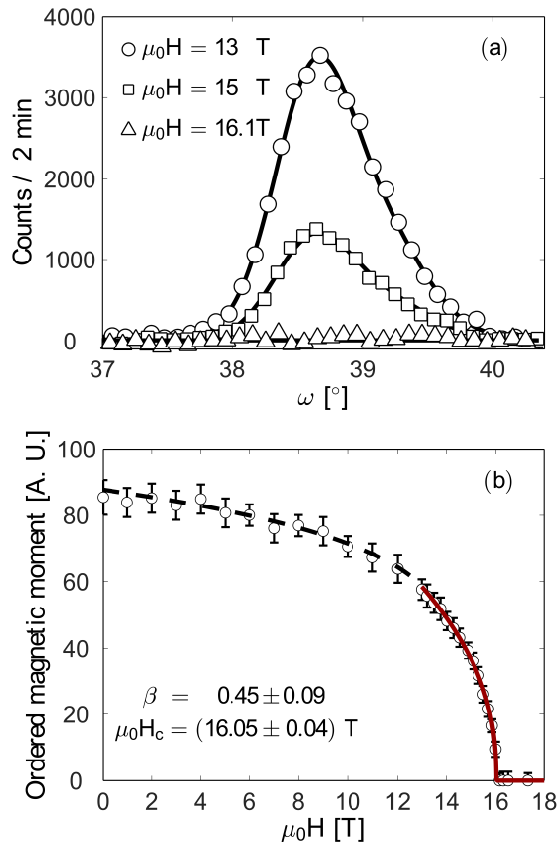
FIG. 2. (a) Examples of raw data for the $\mathbf{Q}_{AFM} = (2\ 1\ 1)$ magnetic Bragg peak. The solid lines represent fits of two Gaussians, as explained in the main text. (b) Square root of the integrated intensity of the Bragg peak as a function of applied field. The solid line is a power law fit. The dashed line is a guide to the eye.

with the ratio $(g_{xx}/g_{yy})^2 \simeq 3.3$ makes it clear that this peak is the x-polarized spin wave. Figure 3 shows constant momentum scans at $\mathbf{Q}_{AFM}$, where the excitation spectrum has its minimum for all fields (see Appendix C). The salient features of the data obtained in finite transverse field are as follows: Upon increasing the field a second sharp Gaussian mode emerges, moves to lower energies and increases in intensity. The sharp mode coexists with a broader field-independent feature around 3.3 meV, which we attribute to an optical phonon mode identified at 3.65 meV in $CoCl_2 \cdot 2H_2O$[16,17]. In deuterated crystals, THz spectroscopy shows that this mode is shifted to energies around 3.3 meV[23].

Figures 4(a)-(e) show the lowest-energy part of the spectrum at $\mathbf{Q}_{AFM}$ for fields close to H_c. From these data, we subtract a model of the incoherent background, measured at $\mathbf{Q} = (1.9\ 1.6\ 0.9)$ (see Fig. 4(e)), to produce the data in Figs. 4(f)-(j). The results show a well-defined excitation decreasing in energy and increasing in intensity for $H < H_c$. At $\mu_0 H = 16$ T (Figs. 4(c) and (h)), very close to the critical field $\mu_0 H_c$, no excitation

is observed. This implies that the mode has completely merged with the elastic incoherent signal in Fig. 4(c). Hence the mode energy at $\mu_0 H = 16$ T is 0 meV within an uncertainty given by the width (HWHM), 0.15 meV, of the incoherent background scattering. In the quantum paramagnetic phase for $H \geq H_c$, the Zeeman term in the Hamiltonian causes a finite energy-cost for spin-flip excitations. As a result, a magnetic excitation reappears and its energy increases with increasing field [Figs. 4(i) and (j)]. The resulting transverse magnetic field dependence of the excitation gap is shown in Fig. 4(k). We observe the theoretically expected complete closure of the excitation gap $\Delta \propto |H_c - H|^{z\nu}$ with the critical exponent close to $z\nu = 1/2$.

IV. DISCUSSION

To understand the evolution of the magnetic excitations, in a manner which accurately treats the strong intrachain interaction, a mean-field/random-phase approximation theory employing a basis of clusters with 3 or 4 spins along the c axis was developed[18] (the methods used in the theory are described in the references[24–26]). The crystal-field parameters of the Co^{2+} ions[14,27] have been adjusted so that the model agrees with the observation of the lowest excited doublet at about 20 meV (see Appendix A). Its proximity to the zero-field spin wave energy range at 4-6 meV[20–22], implies that the excited doublet shifts the spin wave energies by 5-10%. The theory accounts for the bulk properties, i.e. the paramagnetic susceptibility tensor[14] and the low-temperature magnetization curves[13]. Assuming a pure Heisenberg interaction between the spins of the $S = 3/2$ ions, a set of exchange parameters can be derived, which describe not only the zero-field spin waves[20–22], but also the spin reversal excitations (magnon bound states) of clusters of 2, 3, or more neighboring spins along the c-axis chains[16,17], which are neglected by spin wave theory. The parameters and the detailed derivation of the cluster model will be published elsewhere[18].

We now employ the results of the cluster model to understand the data in Figs. 3 and 4. When applying a transverse field along $\mathbf{x}$, the x-polarized mode is predicted to stay roughly constant in energy, whereas its intensity gradually declines. The mode which is y-polarized in zero field becomes an elliptically (yz)-polarized mode. Since $(g_{zz}/g_{xx})^2 \simeq 3.5$ and the angle between the $\mathbf{Q}_{AFM}$ and $\mathbf{z}$ is $\sim 74°$, the z component has a large cross-section, and the (yz)-polarized mode becomes dominant for fields $\mu_0 H \geq 10$ T. The solid line in Fig. 4(k) represents the model predictions as explained in the figure caption. The field dependence of the gap shown in the figure agrees within uncertainties with the theoretical curve demonstrating that there is no experimental evidence for $z\nu$ being different from 1/2.

Next, we compare the critical behavior of $\langle S^z \rangle$ and the excitation gap (Figs. 2(b) and 4(k)) to the TFIC. For this
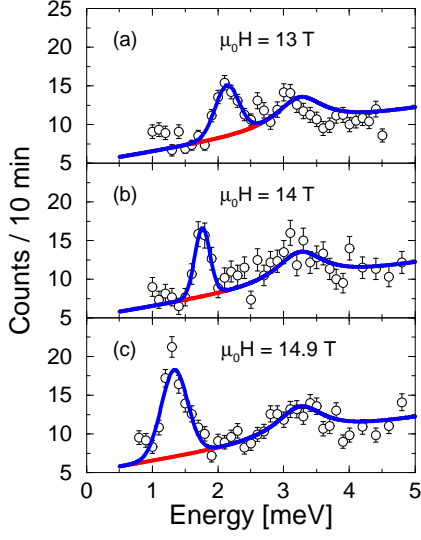
FIG. 3. Raw inelastic neutron scattering data from RITA-II measured at $\mathbf{Q}_{AFM} = (2\,1\,1)$ in transverse fields between 13 T and 14.9 T at $T = 1.5$ K. The blue solid line at each field represent the sum of a Gaussian low-energy magnetic peak and a broad and field-independent contribution that was estimated mainly from the 14.9 T data. The background estimate is shown as red solid lines that overlap with the blue lines at higher energy transfers.
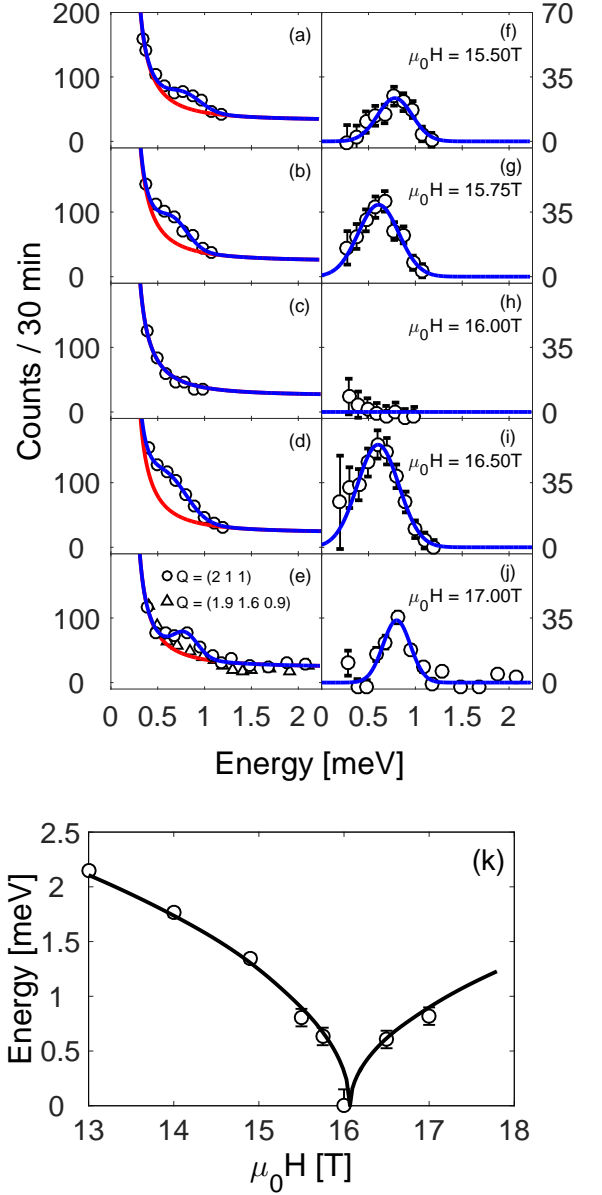

FIG. 4. (a)-(e) Raw inelastic neutron scattering data from FLEXX for transverse fields close to H_c and $T = 1.5$ K. The solid lines are Gaussian fits to the peaks at $\mathbf{Q}_{AFM} = (2\,1\,1)$ assuming a background given by the incoherent scattering at $\mathbf{Q} = (1.9\,1.6\,0.9)$. The latter is shown in panel (e) and represented by the dashed lines in panels (a)-(d). In panels (f)-(j) this background model is subtracted from the raw data. (k) Field dependence of the gap extracted from Gaussian fits to the RITA-II and FLEXX data. The line is calculated using the 4-spin cluster model[18]. The fields in the model calculation were rescaled by about 12% to match the experimentally measured value.

1D model defined by Eq. (1), it is known[1,7] that the quantum critical behavior is given by $\langle S^z \rangle \propto (H_c - H)^\beta$ with $\beta = 1/8$. The well-known quantum-to-classical mapping[1] implies that this β equals the critical exponent characterizing the temperature-dependence of the sublattice magnetization for the classical thermal phase transition of the Ising model in 2D. The prediction $\beta = 1/8$ deviates strongly from the observed value $\beta = 0.45(9)$. Similarly, the experimental result $z\nu \simeq 1/2$ is inconsistent with the value $z\nu = 1$ expected for an ideal TFIC[1,7]. Conversely, a mean-field treatment, e.g. the cluster model we employ, of the Heisenberg model with anisotropic interactions in a transverse field, Eq. (2), would yield the effective critical exponents $\beta = 1/2$ and $z\nu = 1/2$, in good correspondence with our results. This implies that the transverse field QPT in $CoCl_2 \cdot 2D_2O$, which has for decades been regarded as a fair approximation of the TFIC model, Eq. (1), is in fact dominated by mean-field effects.

The major reason for the 3D-like, classical behavior of the QPT in $CoCl_2 \cdot 2D_2O$, i.e. that $\beta \simeq 1/2$, is the size of the effective longitudinal field h^z deriving from the interchain couplings. The interchain interactions are also the major cause of the differences in the excitation spectra observed in this compound and in $CoNb_2O_6$. The anisotropy of the spin interactions is of the same order of magnitude in the two compounds and the values of J_0^z are comparable. However, the ratio between the inter- and intrachain interactions is $h^z/J_0^z = 0.02$ in $CoNb_2O_6$[8] but about $h^z/J_0^z = 0.4$ in $CoCl_2 \cdot 2D_2O$[18]. The relative importance of interchain interactions is also reflected in a large difference between the magnetic ordering temperatures, that T_N is only 2.95 K in $CoNb_2O_6$ but 17.2 K in $CoCl_2 \cdot 2D_2O$.

V. CONCLUSION

In summary, we have observed a transverse-field-induced QPT in the effective $S = 1/2$, quasi-1D anisotropic ferromagnet $CoCl_2 \cdot 2D_2O$ at the critical field of $\mu_0 H_c = 16.05(4)$ T. The QPT is accompanied by a complete closure of the gap in the excitation spectrum at $\mu_0 H_c$. The critical exponents for the sublattice magnetization, $\beta = 0.45(9)$, and for the gap, $z\nu \simeq 1/2$, were found to agree with mean-field theory, but to differ significantly from the predictions for the ideal TFIC model, Eq. (1). These deviations are caused primarily by the finite interchain interactions. The weak 3D nature of the interactions in $CoCl_2 \cdot 2D_2O$ implies that the excitations propagating along the chains consisting of single domain walls are quenched and replaced by excitations of bound pairs of domain walls, i.e. the excitations observed by Torrance and Tinkham[16,17]. The latter are accounted for by the 4-spin cluster theory[18] and have been analyzed in detail by Shinkevich and Syljuåsen[28]. We therefore conclude that the nature of the QPT in $CoCl_2 \cdot 2D_2O$ in a transverse field does not allow us to classify the system as being the $S = 1/2$ ferromagnetic Ising chain considered by Pfeuty[7] and Sachdev[1].

ACKNOWLEDGMENTS

Appendix A: Crystal field levels in $CoCl_2 \cdot 2D_2O$

The higher lying doublet excitations in $CoCl_2 \cdot 2D_2O$ were measured at the direct time-of-flight spectrometer MARI (ISIS, Rutherford Appleton Laboratory, UK). 13.7 g of polycrystalline $CoCl_2 \cdot 2D_2O$ was wrapped in a thin aluminium foil in an annular geometry and thermalized by helium exchange gas. The measurements were performed at 5 K and 100 K using an incident energy of 50 meV with a corresponding (elastic) energy resolution of $\hbar\omega = 1.6$ meV. The data reduction was performed using the Mantid framework[29], which uses standard procedures in order to transform from raw time-of-flight data to the dynamical structure factor $\mathcal{S}(\mathbf{Q}, \hbar\omega)$, where $\mathbf{Q}$ and $\hbar\omega$ are the momentum and energy transfer from the neutrons to the sample.

The results shown in Fig. 5 are the scattering intensities integrated in $\mathbf{Q}$ space over two different volumes. The Q^2 dependence of the phonon cross section implies that the phonons appear with increasing weight, when the radius in $\mathbf{Q}$ space is changed from 4 to 9 Å^{-1}. This circumstance allows the interpretation that the scattering accounted for by the calculated red line, which is more or less unaffected by the change of integration interval, is magnetic, whereas the remaining part, which is roughly changed by a factor of 2 by the change in integration volume, is due to the phonons. We observe one clear magnetic peak at an energy transfer of 21.5 meV at 5 K, which is slightly shifted to 19 meV at 100 K consistent with the calculated behavior. The peak is due to the upper doublet derived from the four $S = 3/2$ spin states belonging to the ground state L level of the Co^{2+} ions.
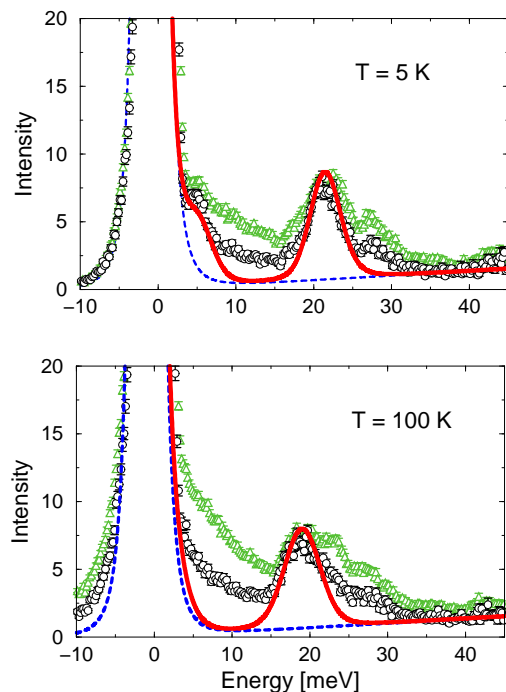

FIG. 5. Data from the MARI experiment, showing the **Q**-integrated intensity vs. energy for two temperatures: 5 K and 100 K. The black circles are the results obtained when integrating the scattering intensity with respect to Q between 0 and 4 Å^{-1}, whereas the blue circles are the results obtained, when integrating from 0 to 9 Å^{-1}. The red solid lines are the calculated results obtained by the mean-field/random-phase approximation theory using a cluster basis of 3 spins along the Co chains and assuming the background scattering shown by the dashed blue lines[18].

Appendix B: Magnetic phase diagram of $CoCl_2 \cdot 2D_2O$ in a transverse magnetic field

To determine the phase diagram of $CoCl_2 \cdot 2D_2O$ in a transverse magnetic field, we recorded the field-dependence of the intensity of the magnetic Bragg peak $\mathbf{Q}_{AFM} = (2\,1\,1)$ at a number of temperatures. This allows us to determine the variation of T_N with the applied field. The resulting phase diagram, which combines data from RITA-II and FLEXX, is shown in Fig. 6.
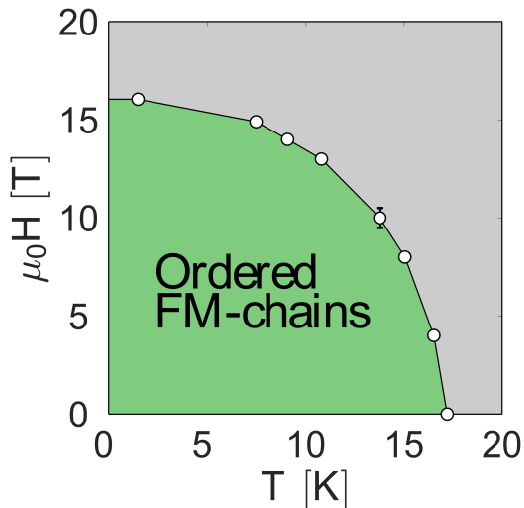

FIG. 6. Magnetic phase diagram of $CoCl_2 \cdot 2D_2O$ in a transverse magnetic field. At low temperatures and fields $CoCl_2 \cdot 2D_2O$ orders antiferromagnetically, as shown in Fig. 1.

Appendix C: Full magnetic dispersion of $CoCl_2 \cdot 2D_2O$ in transverse fields

The full magnetic dispersion relation was measured at the cold-neutron direct geometry time-of-flight spectrometer CNCS at the Spallation Neutron Source, Oak Ridge, Tennessee[30]. We used three co-aligned single crystals of total mass ~ 1 g, oriented as described in the main text with the $(2\,0\,1)$ and $(0\,1\,0)$ axes in the horizontal scattering plane. The sample was inserted in the 16 T vertical field magnet, and we were able to successfully acquire data at 0 T and 12 T transverse field. We used an incident neutron energy $E_i = 12$ meV with the Fermi chopper and the double disc choppers operating at a fre-

quency of 120 Hz and the bandwidth choppers operating at 60 Hz. The data were reduced to $\mathcal{S}(\mathbf{Q}, \hbar\omega)$ using of Mantid[29].

The upper and lower left panels of Fig. 7 show the scattering intensity plotted versus $(h\,0\,h/2)$ and energy transfer $\hbar\omega$. The experimental data are integrated over a range $k = \pm 0.25$ along the in-plane $(0\,k\,0)$ direction. Along the vertical direction, the data are integrated over the full range of momentum transfers allowed by the limited opening angle of the cryomagnet.

Both data sets were obtained at base temperature, $T = 1.5$ K. The 0 T data are consistent with earlier reports[20–22]. At 12 T transverse field, a clear softening of the magnetic mode is seen at $h = 2$, corresponding to $\mathbf{Q}_{AFM}$. The magnetic excitation furthermore appears broadened at $\mathbf{Q}_{AFM}$ at this field. This effect likely represents the splitting of the two spin wave modes predicted by theory[20–22] and reproduced by our theoretical calculations, shown the right panels of Fig. 7.

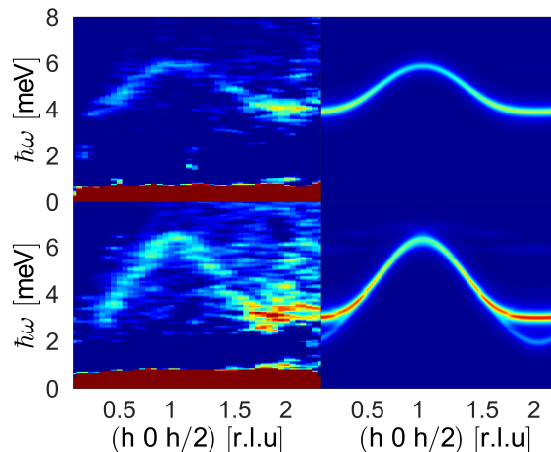

FIG. 7. Data from the CNCS experiment, showing the magnetic dispersion in a $(\mathbf{Q}, \hbar\omega)$-slice with the momentum axis along the $(h\,0\,h/2)$ reciprocal space direction and the neutron energy transfer to the sample, $\hbar\omega$, vectical. The left panels show the measured data in zero field (top) and 12 T (bottom) transverse field. The right panels shows the corresponding correlation functions at $H/H_c = 0$ and 0.75 calculated with in the mean-field/random-phase approximation theory with a cluster basis of 4 spins[18]. To simulate the effect of experimental resolution, the calculated spectra were convoluted with a Lorentzian with an energy-independent width $\Gamma = 0.15$ meV. From this data it is observed that the dispersion softens exactly at $\mathbf{Q}_{AFM}$ $(h = 2)$.

[1] S. Sachdev, *Quantum Phase Transitions*, Cambridge University Press (1999).
[2] M. Greiner, O. Mandel, T. Esslinger, T. W. Hänsch and I. Bloch, Nature **415**, 39 (2002)
[3] J.-H. Chu, H.-H. Kuo, J. G. Analytis, I. R. Fisher, Science **337**, 710 (2012)
[4] D. LeBoeuf, S. Krämer, W. N. Hardy, R. Liang, D. A. Bonn and C. Proust, Nature Physics **9**, 79 (2013)
[5] Ch. Rüegg, A. Furrer, D. Sheptyakov, Th. Strässle, K. W. Krämer, H.-U. Güdel, and L. Mélési, Phys. Rev. Lett. **93**,

257201 (2004)

[6] A. Osterloh, L. Amico, G. Falci and R. Fazio, Nature **416**, 608 (2002)

[7] P. Pfeuty, Annals of Physics **57**, 79 (1970).

[8] R. Coldea, D. A. Tennant, E. M. Wheeler, E. Wawrzynska, D. Prabhakaran, M. Telling, K. Habicht, P. Smeibidl, K. Kiefer, Science **327**, 177 (2010).

[9] I. Cabrera, J. D. Thompson, R. Coldea, D. Prabhakaran, R. I. Bewley, T. Guidi, J. A. Rodriguez-Rivera, and C. Stock, Phys. Rev. B **90**, 014418 (2014).

[10] B. Morosin and E. J. Graeber, Acta. Cryst. **16**, 1176 (1963).

[11] A. Narath, Phys. Rev. **136**, A766 (1964).

[12] D. E. Cox, B. C. Frazer and G. Shirane, Phys. Lett. **17**, 103 (1965).

[13] H. Mollymoto, M. Motokawa, and M. Date, J. Phys. Soc. Japan **49**, 108 (1980).

[14] A. Narath, Phys. Rev. **140**, A552 (1965).

[15] M. Date and M. Motokawa, Phys. Rev. Lett. **16**, 1111 (1966).

[16] J. B. Torrance, Jr. and M. Tinkham, J. Appl. Phys. **39**, 822 (1968).

[17] J. B. Torrance, Jr. and M. Tinkham, Phys. Rev. **187**, 595 (1969).

[18] J. Jensen *et al.* (unpublished)

[19] The angle between $\mu_0\mathbf{H}$ and $\mathbf{x}$ with our alignment is $4.2°$.

[20] J. K. Kjems, J. Als-Nielsen, and H. Fogedby, Phys. Rev. B **12**, 5190 (1975).

[21] N. B. Christensen, K. Lefmann, I. Johannsen, and O. Jørgensen, Physica B **276-278**, 784 (2000).

[22] W. Montfrooij, G. E. Granroth, D. G. Mandrus, and S. E. Nagler, Phys. Rev. B **64**, 134426 (2001).

[23] U. B. Hansen *et al.* (unpublished).

[24] J. Jensen and A. R. Mackintosh, *Rare Earth Magnetism: Structures and Excitations* (Clarendon Press, Oxford, 1991), http://www.nbi.ku.dk/page40667.htm

[25] M. Rotter, M. D. Le, A. T. Boothroyd, and J. A. Blanco, J. Phys.: Condens. Matter **24**, 213201 (2012); http://www.mcphase.de/

[26] J. Jensen, Phys. Rev. B **79**, 014406 (2009).

[27] A. Abragam and M. H. L. Pryce, Proc. R. Soc. Lond. A **206**, 173 (1951).

[28] S. Shinkevich and O. F. Syljuåsen, Phys. Rev. B **85**, 104408 (2012).

[29] O. Arnold, J. C. Bilheux, J. M. Borreguero, A. Buts, S. I. Campbell, L. Chapon, M. Doucet, N. Draper, R. Ferraz Leal, M. A. Gigg, V. E. Lynch, A. Markvardsen, D. J. Mikkelson, R. L. Mikkelson, R. Miller, K. Palmen, P. Parker, G. Passos, T. G. Perring, P. F. Peterson, S. Ren, M. A. Reuter, A. T. Savici, J. W. Taylor, R. J. Taylor, R. Tolchenov, W. Zhou, J. Zikovsky, Nuclear Instruments and Methods in Physics Research Section A: Accelerators, Spectrometers, Detectors and Associated Equipment **764**, 156 (2014); http://www.mantidproject.org/

[30] G. Ehlers, A. A. Podlesnyak, J. L. Niedziela, E. B. Iverson, and P. E. Sokol, Rev. Sci Instr. **82**, 085108 (2011).